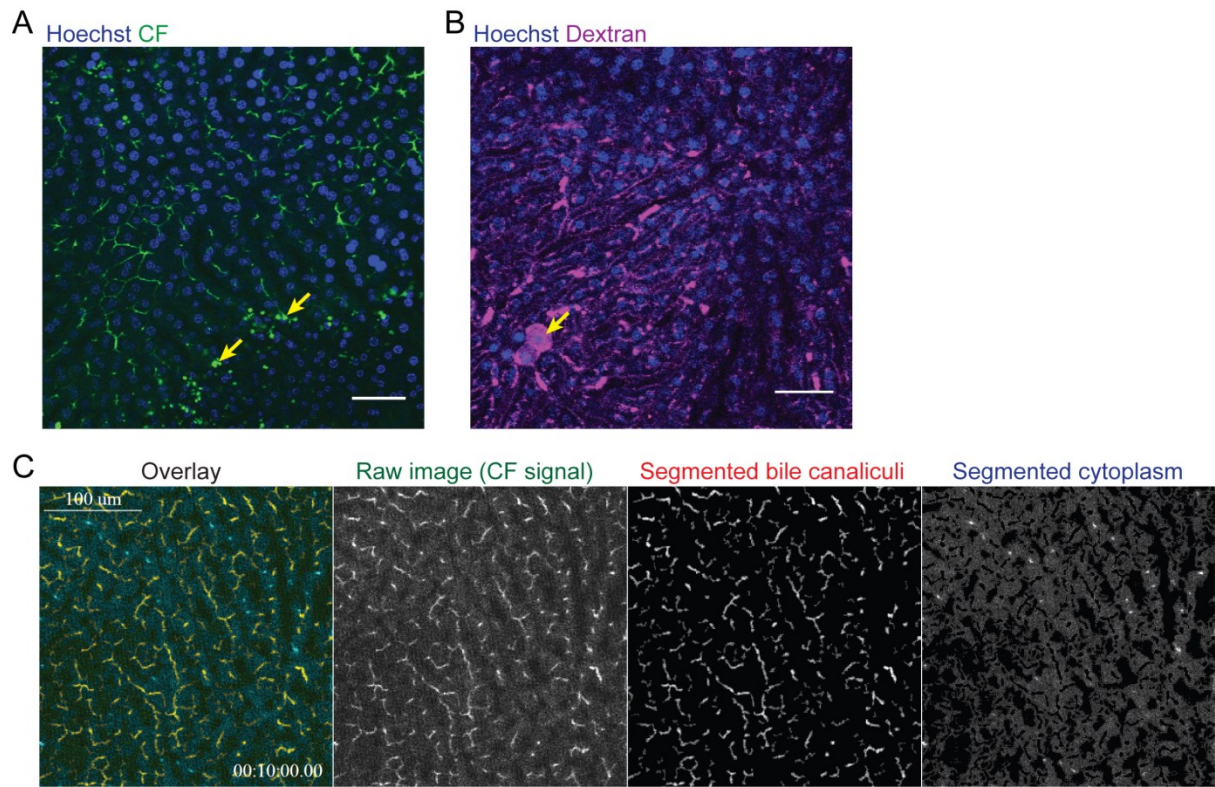


## **Supplemental Information**

## Supplemental Figures

**Figure S1**



**Figure S2**

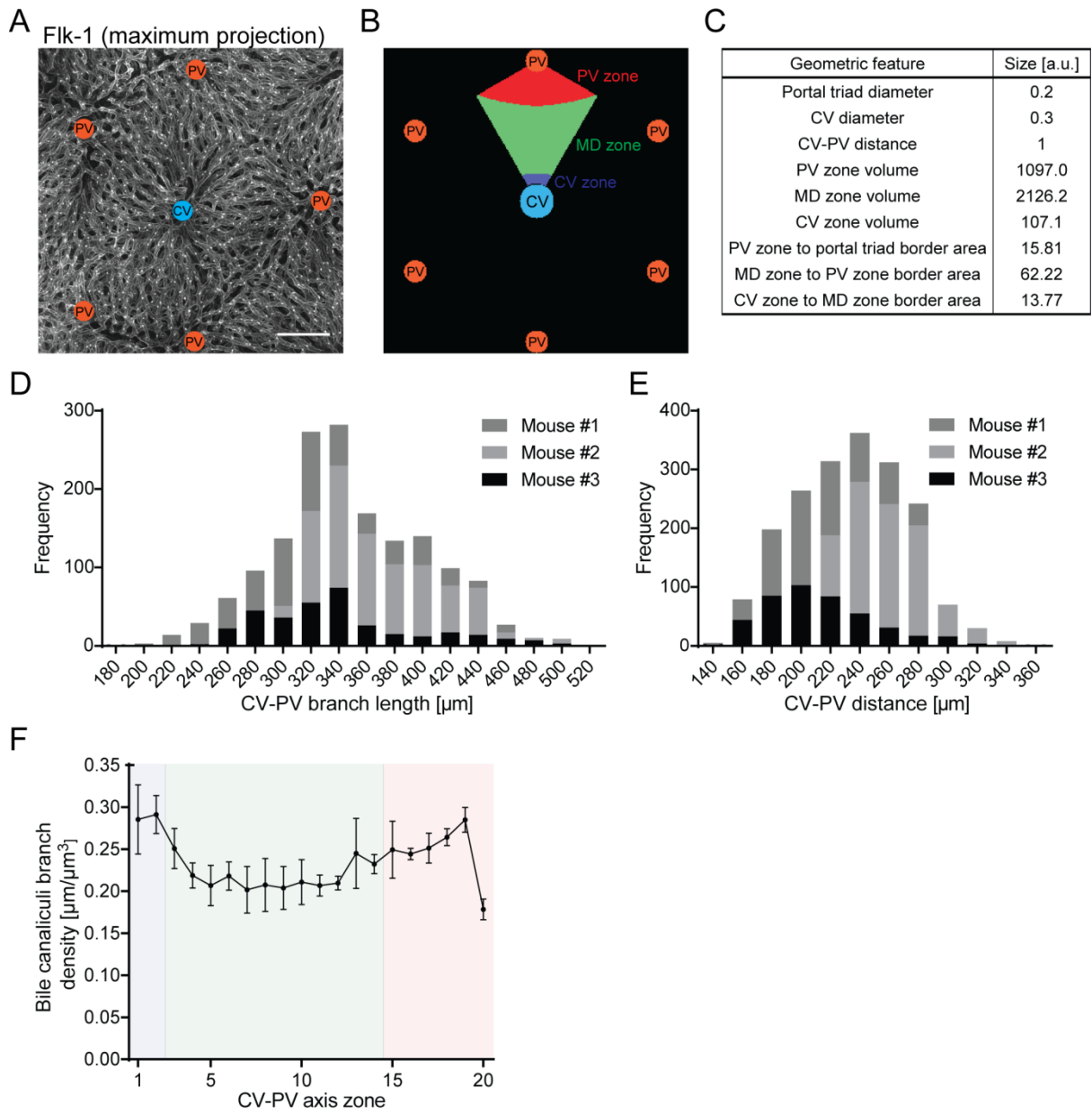
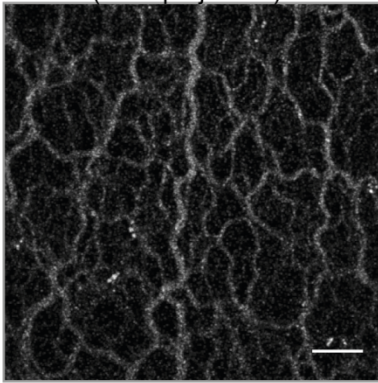


**Figure S3**

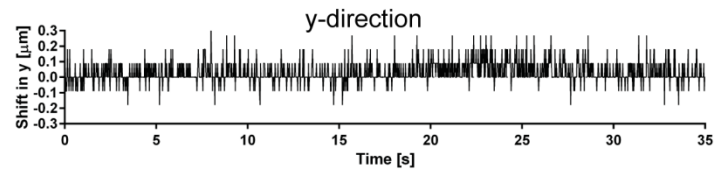
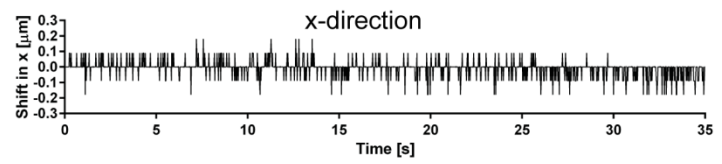
**A** Elastin (Max. projection)



**B** Elastin



**C**



**D**

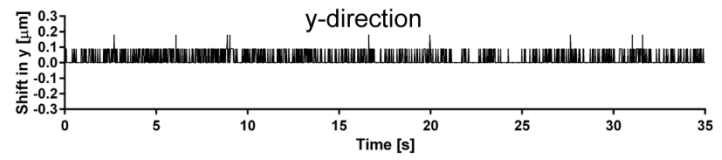
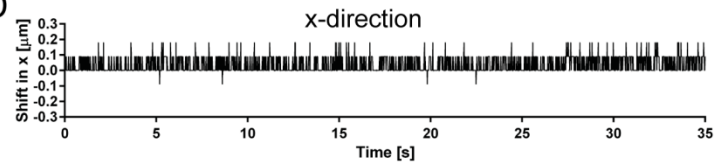


**Figure S4**

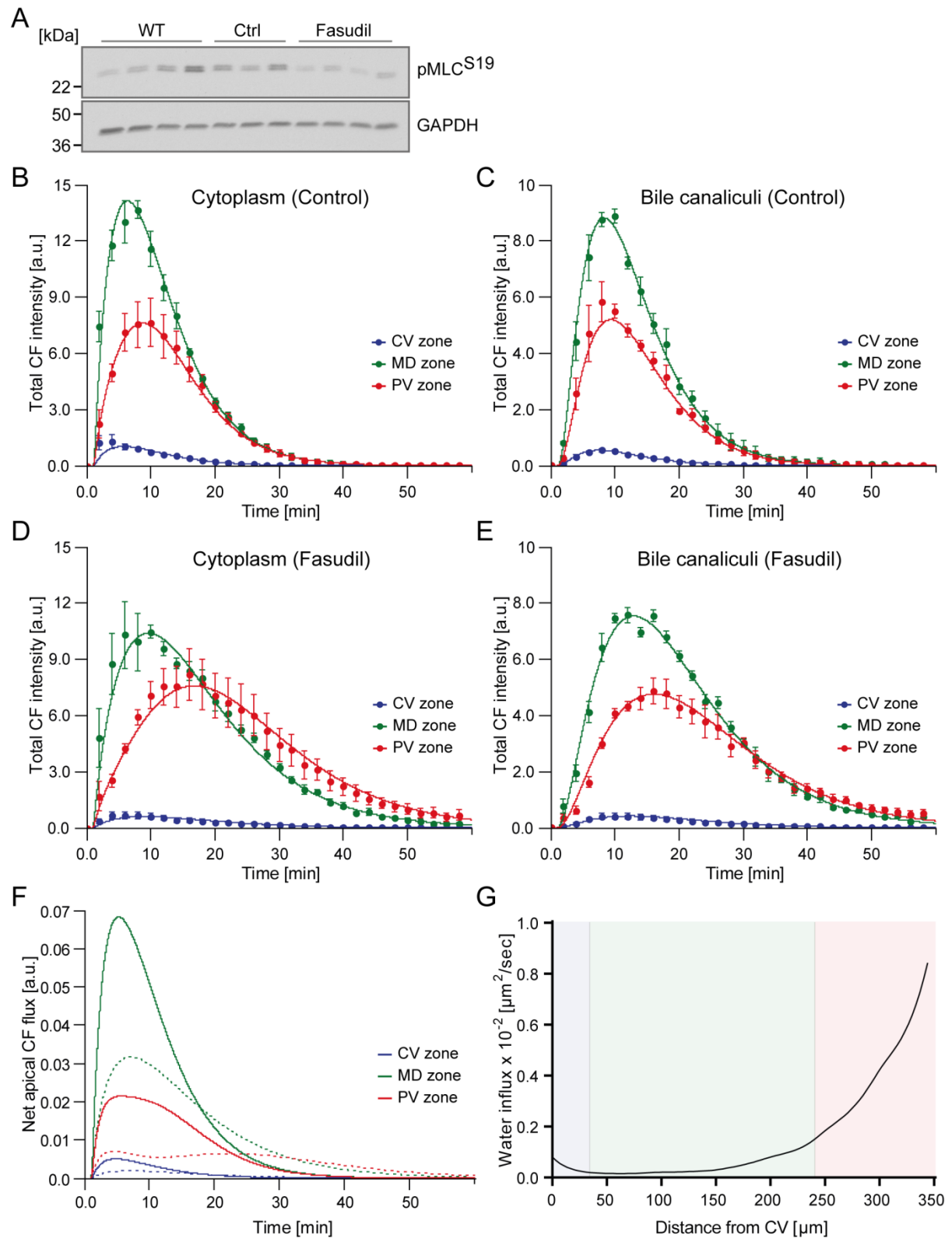
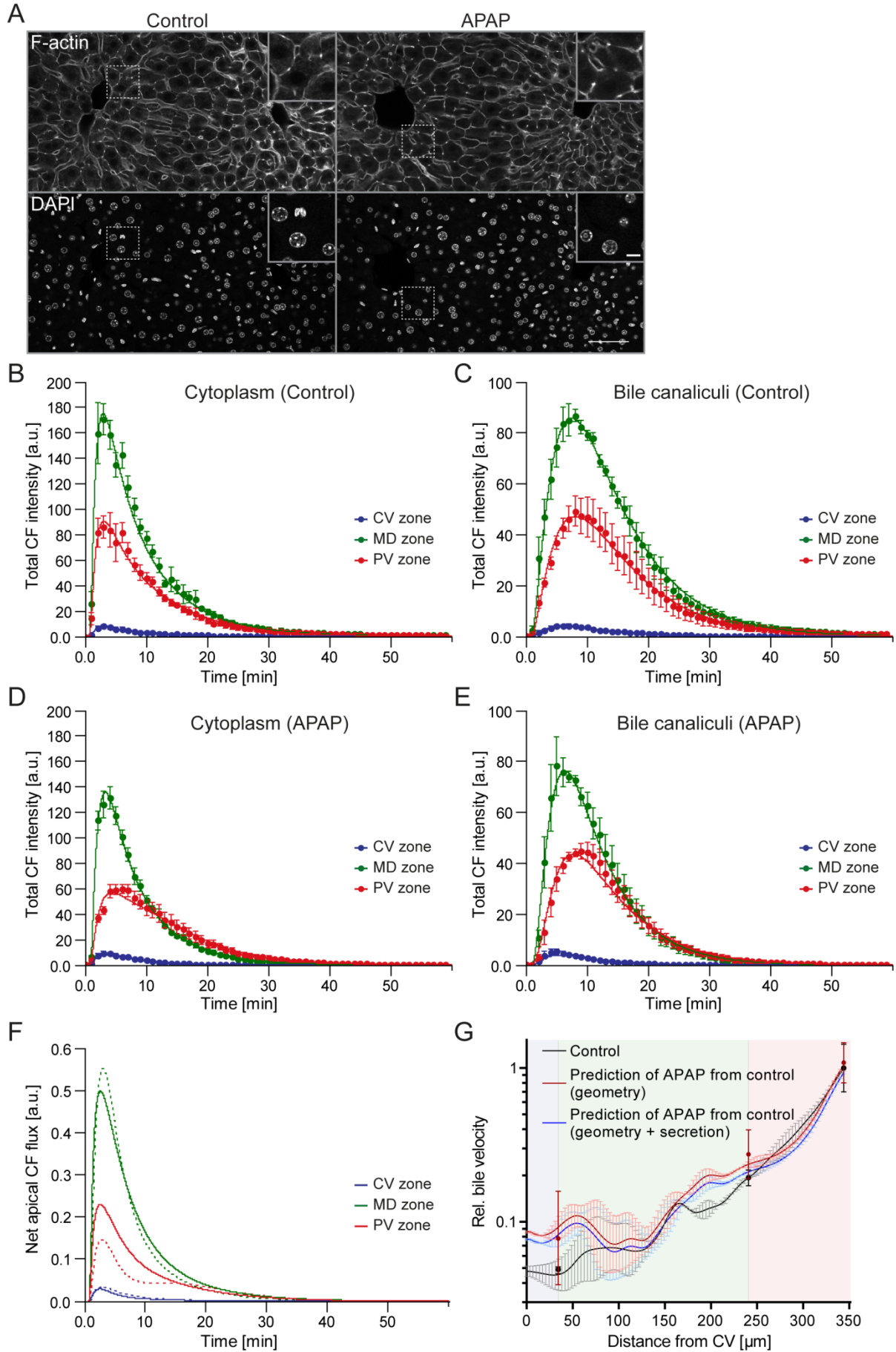


**Figure S5**



## Supplemental Figure legends

### Figure S1 IVM artefacts and image analysis of CF intensity. Related to Figure 2.

**A, B)** Examples of liver tissue damage from IVM of the mouse liver. Arrows show dot-like CF positive structures (A) and cytoplasmic dextran (B) indicating bile canaliculi network fragmentation and compromised hepatocyte plasma membrane integrity, respectively. In the study, IVM movies with indications of tissue damage were excluded from the analysis. **C)** Image segmentation of the cytoplasm and bile canaliculi compartment from IVM movies of CF(DA). Shown is a representative image taken from the middle of a z-stack ( $z = 8 \mu\text{m}$ ) of an IVM movie at time point 10 min, acquired in a Fasudil-treated mouse liver. Shown is an overlay (left image) of the raw image of the CF signal (second image, green on overlay) with the segmentation of the bile canaliculi compartment (third image, red on overlay) and the segmentation of the cytoplasm (fourth image, blue on overlay). Scale bar:  $50 \mu\text{m}$  (A, B),  $100 \mu\text{m}$  (C).

### Figure S2 Geometric properties of the liver lobule. Related to Figure 2 and 6.

**A)** IF staining of a fixed liver tissue section for the sinusoidal marker Flk-1 taken below the liver capsule showing the sinusoid orientation within a lobule. Shown is a maximum projection of a  $87 \mu\text{m}$  z-stack. The approximate localization of the CV (light blue) and PVs (orange) are indicated. **B)** Idealized hexagonal lobule showing the kite-shaped geometry of the CV-PV axis and the geometries of the CV (dark blue), MD (green) and PV zones (red). **C)** Overview of the size of the liver lobule's structural features. Values were determined based on the kite-shaped geometry of an idealized hexagonal lobule as shown in (B). Geometrical units (length, area, volume) are normalized on the CV-PV distance. Therefore, for distances  $1 \text{ a.u.} \approx 300 \mu\text{m}$ , for areas  $1 \text{ a.u.} \approx 9 \cdot 10^4 \mu\text{m}^2$ , for volumes  $1 \text{ a.u.} \approx 2.7 \cdot 10^7 \mu\text{m}^3$ . **D, E)** Quantification of the shortest bile canaliculi network path length (D) and the direct distance (E) between the CV and PV from 3D reconstructions of the bile canaliculi network. Shown are cumulative distributions from 3 mice. **F)** Quantification of bile canaliculi branch density from bile canaliculi network reconstructions as representatively shown in Figure 3B. Quantification was performed for 20 equidistant zones along the CV-PV axis. Zone 1 and 20 are adjacent to the CV and PV, respectively, and displayed on the x-axis. The blue, green and red background indicates the localization of the CV, MD and PV zones, respectively.  $n = 3$  mice, mean  $\pm$  SEM. Scale bar:  $100 \mu\text{m}$  (A).

### Figure S3 Stability of the IVM imaging setup. Related to Figure 5.

**A)** Representative IVM image of elastin fibres of the liver capsule detected by SHG. Shown is a maximum projection of a  $10 \mu\text{m}$  z-stack. **B)** Representative image of elastin fibres from an IVM movie sequence acquired in the same mouse and with the same spatial and temporal resolution as the IVM movie of bile canaliculi contractility shown in Figure 5A and Movie S2. **C, D)** Quantification of the image shift in the x- and y-direction of the movie of elastin fibres shown as still image in B (C) or from an IVM movie of elastin fibres acquired in another mouse at higher temporal resolution (D). Scale bar:  $20 \mu\text{m}$  (A),  $5 \mu\text{m}$  (B).

### Figure S4 Quantification and prediction of CF(DA) transport and osmotic water influx into the bile canaliculi network upon Fasudil treatment. Related to Figure 5.

**A)** Western blot of liver lysates from wild type (WT), control (Ctrl) and Fasudil-treated mice for phospho-myosin light chain (pMLC) and glyceraldehyde 3-phosphate dehydrogenase (GAPDH) from 3-4 mice per condition. Molecular weights (kDa) are indicated. **B-E)** Quantification and model fit of the CF intensities in the hepatocyte cytoplasm (B,D) and bile canaliculi (C,E) from IVM movies of control (B,C) and Fasudil-treated (D,E) mice. Values were determined for the CV (blue), MD (green) and PV (red) zones of the liver

lobule. CFDA was injected at 1 min. Dots represent experimental measurements, solid lines show the fit of the 3-compartment model of CF(DA) transport.  $n = 4$  mice (control),  $n = 5$  mice (Fasudil), mean  $\pm$  68 % CI. a.u., arbitrary units of intensity. **F**) Prediction of the net apical flux of CF in control (solid lines) and Fasudil-treated mice (dashed lines) over the timecourse of imaging of CFDA transport. Values were estimated from the 3-compartment model of CF(DA) transport and represent the difference between apical CF secretion and passive CF back flux into the cytoplasm for the CV (blue), MD (green) and PV (red) zones. a.u., arbitrary units of intensity. **G**) Prediction of the water influx profile into the bile canaliculi network in WT mice from the model of osmotic fluid secretion, corrected for the contribution of peristalsis to bile flow. The blue, green and red backgrounds indicate the localization of the CV, MD and PV zones, respectively.

**Figure S5 Quantification and prediction of CF(DA) transport and bile flow upon APAP treatment. Related to Figure 7.**

**A**) Representative IF images of an entire CV-PV axis of fixed liver sections from control and APAP-treated mice stained for F-actin and nuclei (DAPI). The CV is oriented to the left and PV to the right. Indicated regions (white rectangles) are shown as insets. **B-E**) Quantification and model fit of CF intensity in the hepatocyte cytoplasm (B,D) and bile canaliculi (C,E) for the CV (blue), MD (green) and PV (red) zones from IVM movies of control (B,C) and APAP-treated (D,E) mice. Dots represent experimental measurements, solid lines show the fit of the 3-compartment model of CF(DA) transport (see Figure 2F). CFDA was injected at 1 min.  $n = 4$  mice (control),  $n = 5$  mice (APAP), mean  $\pm$  68 % CI. a.u., arbitrary units of intensity. **F**) Prediction of the net apical flux of CF in control (solid lines) and APAP-treated mice (dashed lines) over the timecourse of imaging of CF(DA) transport. Values were estimated from the compartment model of CF(DA) transport and represent the difference between apical CF secretion and passive CF back flux into the cytoplasm for the CV (blue), MD (green) and PV (red) zones. a.u., arbitrary units of intensity. **G**) Shown is the same graph as in Figure 7D but with addition of the prediction of bile velocity from the model of osmotic fluid secretion and peristalsis considering both the bile canaliculi radius profile and apical secretion rates of CF measured in APAP-treated animals (blue solid line). Dots represent experimental, mean  $\pm$  95 % CI. Solid lines represent model predictions. Error bars of the model predictions were propagated from the SEM of the radius profiles shown in Figure 7B and extrapolated across the CV-PV axis. For detailed description see Figure 7. The blue, green and red backgrounds indicate the localization of the CV, MD and PV zones, respectively. Scale bar in (A): 50  $\mu$ m or 10  $\mu$ m (inset).

## Supplemental Tables

**Table S1 Properties of hepatic CF(DA) transport in wild type, control and Fasudil or APAP-treated mice. Related to Figure 2, 5 and 7.**

Global parameters	WT	Fasudil control	Fasudil	APAP control	APAP
Systemic CFDA clearance ( $k_{clear}$ )	0.016 (0.010-0.025)	0.004 (0.003-0.005)	0.003 (0.002-0.004)	0.020 (0.019-0.021)	0.014 (0.007-0.028)
CFDA cleavage rate ( $k_{cleav}$ )	3.281 (1.478-7.281)	0.142 (0.055-0.369)	0.089 (0.041-0.194)	2.995 (2.515-3.567)	1.922 (0.303-12.200)
Apical transporter activity ( $k_{pump}$ )	0.003 (0.002-0.003)	0.007 (0.005-0.009)	0.005 (0.004-0.006)	0.005 (0.003-0.006)	0.005 (0.002-0.013)

Spatial parameters	Zone	WT	Fasudil control	Fasudil	APAP control	APAP
Rel. esterase density (q)	CV zone	171.63 (52.02-566.27)	58.44 (35.86-95.25)	22.38 (14.12-35.47)	6.72 (5.26-8.59)	110.32 (24.01-506.88)
Rel. apical transporter density (q1)		2.07 (0.93-4.62)	198.52 (32.00-1231.46)*	198.52 (107.20-363.30)*	198.52 (40.37-976.25)*	198.52 (109.19-361.31)*
Apical CF back flux rate ( $k_i$ )		0.00	0.0040 (0.0004-0.0371)	0.0025 (0.0016-0.0039)	0.0025 (0.0015-0.0040)	0.0025 (0.0012-0.0053)
Rel. esterase density (q)	MD zone	1.00 (0.31-3.28)	1.00 (0.28-3.55)	1.00 (0.32-3.09)	1.00 (0.64-1.55)	1.00 (0.13-7.51)
Rel. apical transporter density (q1)		1.00 (0.59-1.69)	1.00 (0.22-4.65)	1.00 (0.21-4.87)	1.00 (0.31-3.19)	1.00 (0.21-4.80)
Apical CF back flux rate ( $k_i$ )		0.0002 (0.0000-0.0019)	0.0034 (0.0009-0.0129)	0.0027 (0.0016-0.0045)	0.0013 (0.0007-0.0027)	0.0017 (0.0005-0.0054)
Rel. esterase density (q)	PV zone	0.68 (0.31-1.49)	0.98 (0.68-1.42)	1.02 (0.59-1.79)	1.18 (0.74-1.88)	0.38 (0.15-0.99)
Rel. apical transporter density (q1)		0.73 (0.24-2.28)	0.10 (0.07-0.14)	0.10 (0.02-0.56)	0.79 (0.30-2.05)	0.10 (0.03-0.30)
Apical CF back flux rate ( $k_i$ )		0.0004 (0.0001-0.0011)	0.0045 (0.0015-0.0136)	0.0054 (0.0027-0.0109)	0.0016 (0.0009-0.0031)	0.0031 (0.0012-0.0079)

Estimate of CF(DA) transport properties obtained by fitting the 3-compartment model of CFDA transport to experimental measurements of CF flux from IVM movies in wild type (WT), Fasudil control, Fasudil, acetaminophen (APAP) control and APAP-treated animals. Parameters correspond to the rate constants of the compartment model of CFDA transport, shown in Figure 2F (see also STAR Methods). Shown are mean values from 4-5 mice per condition and the 95 % confidence interval in brackets. The density of esterase and transporter was determined based on the kite-shaped geometry of the CV-PV axis (see Figure S2C). Parameters expressed as relative values were normalized to the MD zone. \* The model has low sensitivity to the given parameter.

**Table S2 Overview of parameters of the model of osmotic fluid secretion (and peristalsis). Related to Figure 4, 5 and 7.**

Condition	Relation to Figure	$p_1$ [1/ $\mu\text{m}$ ]	$p_2$ [ $\mu\text{m}$ ]
WT	4C – Fit of bile velocity	824.3 [1/sec]	$10.11 \cdot 10^{-6}$
	S4G – Prediction of water influx profile	824.3 [1/sec]	$10.11 \cdot 10^{-6}$
Fasudil	5E – Fit of Control	566.9	$6.656 \cdot 10^{-6}$
	5E – Prediction of Fasudil from control	379.7	$6.656 \cdot 10^{-6}$
	5E – Fit of Fasudil	230.1	$6.970 \cdot 10^{-6}$
	5E – Prediction of control from Fasudil	343.6	$6.970 \cdot 10^{-6}$
APAP	7D – Fit of Control	395.6	$5.476 \cdot 10^{-6}$
	7D – Prediction of APAP from control	409.0	$5.476 \cdot 10^{-6}$

Overview of the parameters applied to fit and predict bile velocity from the model of osmotic fluid secretion (and peristalsis) for the indicated conditions.  $p_1$ ,  $p_2$ , model parameters fitted or predicted as specified; Units in the header apply unless specified otherwise in the cell.

## **Supplemental Movie legends**

### **Movie S1, Related to Figure 2**

IVM movie of CF(DA) transport in the WT mouse liver. The CV-PV axis is oriented as indicated in Figure 2B. CFDA was injected 1 min after acquisition start. Scale bar, 20  $\mu\text{m}$ .

### **Movie S2, Related to Figure 5**

IVM movie of bile canaliculus contractility in a Lifeact-EGFP mouse liver shown as still images in Figure 5A. Scale bar 2  $\mu\text{m}$ .

### **Movie S3, Related to Figure 5**

IVM movie of CF(DA) transport in the liver of control and Fasudil-treated mice. CV-PV axis is oriented as indicated in Figure 5D. CFDA was injected at 1 min. Scale bar, 25  $\mu\text{m}$ .

### **Movie S4, Related to Figure 7**

IVM movie of CF(DA) transport in the liver of control and APAP-treated mice. CV-PV axis is oriented as indicated in Figure 7C. CFDA was injected at 1 min. Scale bar, 25  $\mu\text{m}$ .